Direct spectroscopic observation of multiple-charged-ion acceleration by an intense femtosecond-pulse laser

A. G. Zhidkov,[1] A. Sasaki,[1] T. Tajima,[1,*] T. Auguste,[2] P. D'Olivera,[2] S. Hulin,[2] P. Monot,[2] A. Ya. Faenov,[3] T. A. Pikuz,[3] and I. Yu. Skobelev[3]

[1]*Advance Photon Research Center, JAERI, 25-1 Mii-minami-cho, Neyagawa-shi, Osaka 572, Japan*

[2]*Commissariat a l'Energie Atomique, Centre D'Etudes de Saclay, DRECAM, Service de Photons Atomes et Molecules, Batiment 522, 91191 Gif-Sur-Yvette, France*

[3]*Multicharged Ions Spectra Data Center of VNIIFTRI, Mendeleevo, Moscow Region 141570, Russia*

(Received 5 April 1999)

We have observed evidence of the emission of energetic He-and H-like ions of fluorine more than 1 MeV produced via the optical field ionization (OFI) from a solid target irradiated by an intense $I=(2-4)\times 10^{18}$ W/cm^2 (60 fs, $\lambda=800$ nm), obliquely incident *p*-polarized pulse laser. The measured blue wing of He_α, He_β, and Ly_α lines of fluorine shows a feature of the Doppler-shifted spectrum due to the self-similar ion expansion dominated by superthermal electrons with the temperature $T_h\sim 100$ keV. Using a collisional particle-in-cell simulation, which incorporates the nonlocal-thermodynamic-equilibrium ionization including OFI, we have obtained the plasma temperature, line shape, and maximal energy of accelerated ions, which agree well with those determined from the experimental spectra. The red wing of ion spectra gives the temperature of bulk plasma electrons. [S1063-651X(99)05009-6]

PACS number(s): 52.40.Nk, 52.50.−b, 41.75.Jv

I. INTRODUCTION

Plasmas with extreme parameters produced by very intense short pulse lasers are being intensively studied for the last decade as sources of energetic particles from x- and γ-ray photons to MeV multiple-charged ions and positrons [1–9]. For ion acceleration, several experiments have indicated emission of energetic ions [7–9]. Thus, characterization of ions through measurements such as their energy distribution and comparison with the theory and calculation are extremely important to clarify the mechanism of ion acceleration as well as to determine future prospect of its application. For measurements of plasma conditions such as temperature and density, time and space resolved x-ray spectroscopy of multiple-charged ions is very informative [2]. In this paper, we demonstrate the possibility of using the Doppler-shifted spectrum of multiple-charged ions for direct measurement of energetic ion emission from short-pulse laser-produced plasmas.

At high laser intensities $I\lambda^2>10^{18}$ W μm^2/cm^2, a considerable portion of the absorbed laser energy is coupled to the emission of energetic ions [3–7]. First, energetic electrons are produced through nonlinear interaction between intense laser and plasma, which create strong electrostatic field on the surface of the plasma to drive its fast expansion. The energy distribution function of ions and efficiency reflect the conditions of short-pulse laser-produced plasmas. Among this, the ionization process on the target surface becomes important for dynamics and kinetics of the plasma. It has been predicted that optical field ionization (OFI) and plasma-induced field ionization can have an effect on the energetic ion emission [6] via enhancement of charges of accelerated ions in the low-density corona plasma where collisional ionization is not efficient. To understand the ion emission process and its role in the plasma energy balance, a direct measurement of the ion charge and ion energy distributions are needed. In this paper, a first direct time-integrated spectroscopic measurement of multiple-charged-ion acceleration from a solid plasma irradiated by a femtosecond-pulse laser is reported. A clear blue wing in the spectrum lines of the $3p$-$1s$, $2p$-$1s$ of He-like and $2p$-$1s$ of H-like ions of fluorine in the direction of plasma expansion are observed. The result displays the presence of MeV ions in the plasma corona with a distribution $N\sim\exp(-v/C_S)$, with the ion sound velocity C_S determined by the superthermal electrons of about 100-keV temperature. This agrees well with the results of a collisional particle-in-cell (PIC) simulation also given below.

II. EXPERIMENT

The experiments were performed with the UHI10 laser [10,11], which was designed to generate 10-TW ultrashort pulses (60 fs) at 10 Hz. It employs the standard chirped-pulse-amplification technique. Titanium-Sapphire rods are used as a laser medium and the operating wavelength of the system is 790 nm. In order to produce such high-power ultrashort pulses with a good contrast, first, the low-energy ultrashort pulse (linear *p* polarized) is stretched up to 300 ps by an aberration-free Offner stretcher. The pulse energy is about 1.8 J after four stages of amplification. Second, the compression is performed in a vacuum chamber directly connected to the experimental chamber. The contrast, measured with a high dynamic cross correlator is about 10^{-5} at 1 ps. The post and prepulses amplitudes are less than 10^{-5}. Total energy in the laser pulse was about 800 mJ. The 80-mm diameter laser beam was focused with an $f/2.35$ off-axis

*Present address: Lawrence Livermore National Laboratory, L-441 Livermore, CA 94551.

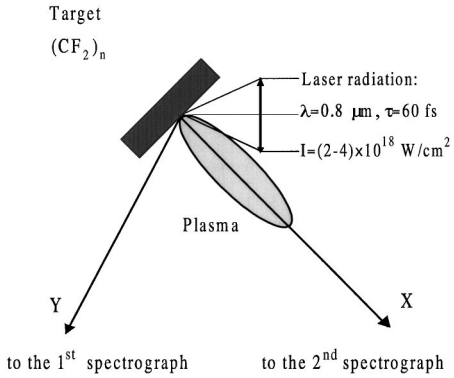

FIG. 1. Scheme of the experiment.

parabolic mirror onto a solid teflon $(CF_2)_n$ target, which was placed at 45° to the direction of the incident laser. The $1/e^2$ focal spot radius measured in vacuum was about 20–30 μm, giving a laser intensity on the target $(2-4)\times10^{18}$ W/cm^2, respectively.

The diagnostic setup is shown in Fig. 1. Spatially resolved x-ray spectra of fluorine in the 13.7–17.2-Å spectral range were obtained using the focusing spectrometer with spatial resolution—two-dimensional [12–15]. Two large aperture (15×50 mm) spherically bent mica (2D in the first order of reflection is about 19.91 Å) crystals with a 150-mm radius of curvature were placed in different experiments at the distances 250–290 mm from the plasma. They covered Bragg angles from 30° up to 46° that allowed us to receive spectra of He-like ions (F VIII) and Ly_α of H-like (F IX}. Theoretical spectral resolution $\lambda/\delta\lambda$ for such a type of spectrometer geometry could be more than 10 000, but in the experiment reported herein it was limited to about 2000–3000, due to the limitation of the rocking curve of the crystal for such long wavelengths [16]. The first spectrometer was mounted in such way (10° to the target surface) that spectrally resolved x-ray images were obtained in the direction of propagation of the laser with about a 20-μm spatial resolution due to the focusing properties of spherically bent crystal. The second spectrometer had spatial resolution along the target surface and was placed perpendicular (90°) to the target surface (see Fig. 1). Spectra were recorded on RAR 2492 film. The film holder was protected by two layers of 0.8-μm polypropylene filters coated with 0.2 μm of Al on both sides.

The results of a time-integrated measurement of H_α, He_α, and He_β line spectra of fluorine are shown in Figs. 2–4. All spectra recorded in the direction perpendicular to the target surface show a strong asymmetrical feature in contrast to the spectra recorded in the direction parallel to the target surface. We believe that the blue wing of the spectra are produced by Doppler-shifted radiation of energetic ions emitted from the target. From the theory of long pulse laser and plasma interaction and numerical simulation it is well known that ions are accelerated over MeV by an electrostatic field generated by superthermal electrons [17]. We make an estimation of hot electron temperature in the plasma assuming that the velocity distribution of ions under such acceleration is close to the self-similar distribution [18],

$$N(v)\approx N_0\exp(-v/C_S), \tag{1}$$

where $C_s=(ZT/M_i)^{1/2}$ is the ion sound velocity with T electron temperature, Z and M_i are the charge and mass of ions, respectively. The Doppler line shape for the distribution of Eq. (1) has the following form,

$$S(\lambda-\lambda_0)\propto\exp(-|\lambda-\lambda_0|/\lambda_S), \tag{2}$$

where $\lambda_s=\lambda_0 C_S/c$. Upon fitting the He_α and He_β spectral lines by distribution (2) with λ_s as a parameter, we can determine the ion sound speed for the blue and red parts of the

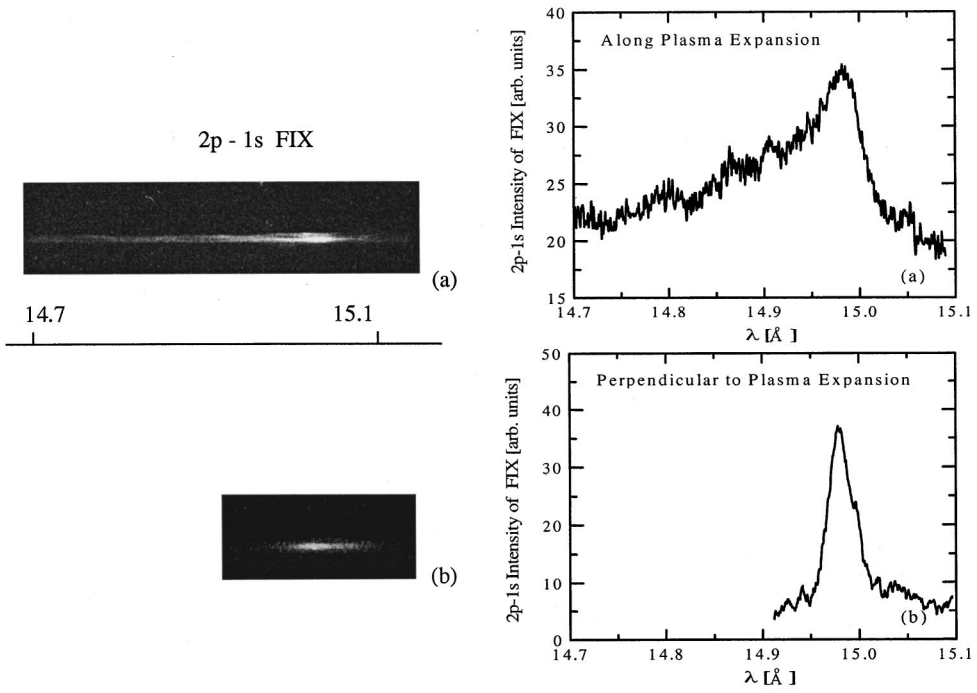

FIG. 2. Time-integrated spectral intensity of the $2p$-$1s$ line of H-like fluorine ions (a) parallel and (b) perpendicular to the target surface.

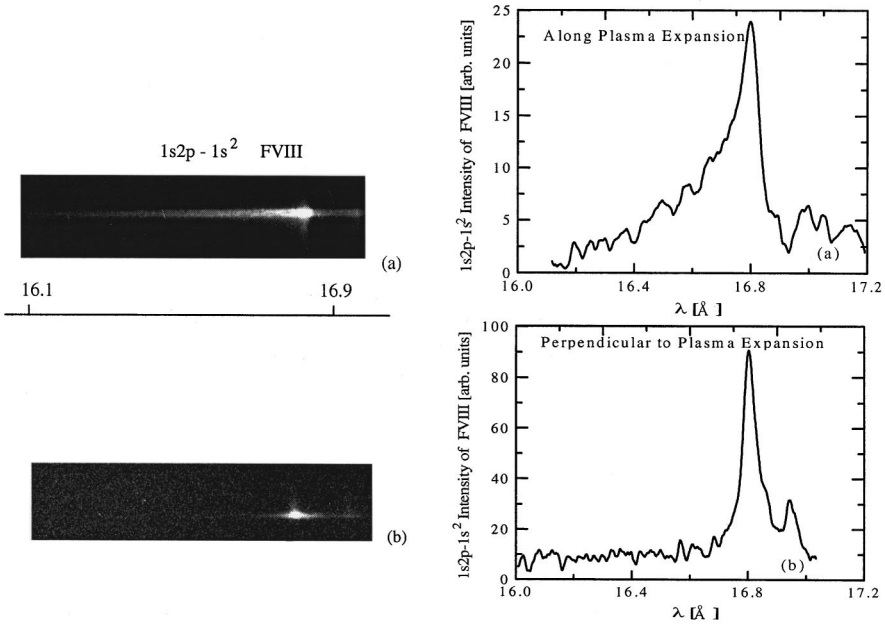

FIG. 3. Time-integrated spectral intensity of the $1s2p$-$1s^2$ line of He-like fluorine ions (a) parallel and (b) perpendicular to the target surface.

spectra and then the temperature of electrons dominating plasma expansion. Thus from the blue part of the spectra we find $T_B(\mathrm{He}_\alpha)=105\,\mathrm{keV}$ and $T_B(\mathrm{He}_\beta)=112\,\mathrm{keV}$. These agree well with the temperature of the superthermal electrons followed from the well-known approximation [19,20],

$$T_h=30(I\lambda^2/10^{17}\ \ \mathrm{W}\,\mu\mathrm{m}^2/\mathrm{cm}^2)^{1/3}(T_c,\ \ \mathrm{keV})^{1/3}\ \ \mathrm{in\,keV},$$

where T_c is the temperature of the bulk plasma. This equation gives $T_h=110\,\mathrm{keV}$ for the laser parameters above. The same procedure for the red part of the spectra and for the spectra recorded along the target surface gives the temperature $T_R=1.5-2\,\mathrm{keV}$, which might correspond to the bulk plasma temperature T_c.

III. CALCULATION

To reveal the process of ion acceleration under a short pulse laser, we employ a method based on the collisional electromagnetic PIC to explore the dynamics of a solid density fluorine plasma irradiated by a femtosecond *p*-polarized, obliquely incident pulse laser. The method incorporates the Langevin equation to account for elastic collisions and the non-LTE average ion model for plasma ionization including the ionization due to the laser as well as plasma field. The method conforms to a direct solution of the Fokker-Planck equation. The details of the method can be found in [21]. To solve the Maxwell equations, we use the two waves approximation [21]. In this way we correctly treat the collisional absorption, vacuum heating, anomalous skin effect, and resonance absorption for an obliquely incident laser pulse in the laboratory reference frame. We include ionization processes in the PIC simulation by allowing the change of computational particle (CP) charges. A change in the charge of CP's representing plasma electrons is calculated by the standard electron balance equation in a ''kinetics'' cell, which includes many cells. The OFI is included as a process of suc-

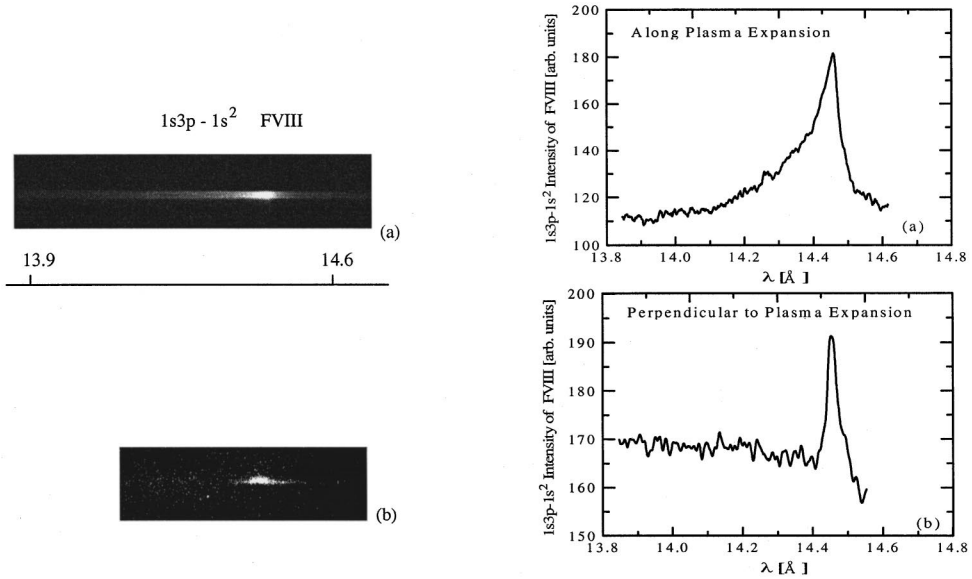

FIG. 4. Time-integrated spectral intensity of the $1s3p$-$1s^2$ line of He-like fluorine ions (a) parallel and (b) perpendicular to the target surface.

cessive ionization whose probability depends on the electric field strength E and ionization potential of the average ion I_Z in a ''kinetics'' cell according to [22,23]

$$\nu_E = 4\omega_A (I_Z)^{5/2} \frac{E_A}{E_L} \exp\left(-\frac{2}{3}(I_Z)^{3/2} \frac{E_A}{E_L} \right), \tag{3}$$

where I_Z is the ionization potential in Ry for an ion, $E_A = m^2e^5/\hbar^4$, $\omega_A = me^4/\hbar^3$, and E_L is the laser field strength. To conserve energy, we add the effective atomic current $\mathbf{j}_A$ to the Maxwell equations following [24] and assuming that the Ohmic heating due to this current must be equal to the energy loss for the field ionization,

$$\mathbf{j}_A \mathbf{E} = \sigma_A E^2 = I_{Z+1} \nu(I_{Z+1}, E) N_Z, \tag{4}$$

where σ_A is an effective atomic conductivity and ν is the field ionization probability. The current components are calculated then as $\mathbf{j}_A = \sigma_A \mathbf{E}$. The atomic current is used self-consistently in the Maxwell equations along with the plasma current. The average charge of every CP representing ions is used in the equation of motion.

The 1–2/2D relativistic electromagnetic PIC code with the square current and charge weighting is used to calculate the interaction of an intense obliquely incident *p*-polarized-pulse laser with a solid plasma. Collisions are computed as an effective force after calculation of the velocity and position of CPs. The calculation with movable ions is carried out for the fluorinelike solid target with the stepwise initial density distribution. The initial temperature of the plasma is 10 eV, the ion charge $Z=1$, and $N_0 = N_e = N_i = 5\times10^{22}\,\mathrm{cm}^{-3}$. The laser intensity $I=(1-4)\times10^{18}\,\mathrm{W/cm^2}$, at $\lambda = 800\,\mathrm{nm}$ (maximal $eE_0/m\omega c$ is equal to 0.9), is chosen to be constant during the laser pulse, and the pulse duration is 60 fs. The time step is set to $0.03/\omega_{\mathrm{pl}}^0$, where ω_{pl}^0 is the initial plasma frequency. The number of CP's is $N=5\times10^4$ per 1 μm of the plasma. Two boundary conditions are used at the shaded side of a simulation box of 4-μm length. First is the total absorption of particle energy at the boundary and the second corresponds to a foil with a thickness of 2 μm.

We find that the absorption efficiency of the 60-fs pulse laser is about 12% at intensity $I=10^{18}\,\mathrm{W/cm^2}$ and about 10% at $4\times10^{18}\,\mathrm{W/cm^2}$ on a solid target. This increases up to 18 and 15% for a foil with thickness of 2 μm, respectively. The vacuum heating, constrained by the ponderomotive force, dominates the absorption rate [25]. Plasma parameters at (a) $I=2\times10^{18}\,\mathrm{W/cm^2}$ and (b) $I=4\times10^{18}\,\mathrm{W/cm^2}$ after the laser pulse (after 60 fs) are presented in Figs. 5 and 6. (In the following figures, electron and ion densities are measured in N_0.) The spatial distribution of the ion density and charges are presented in Fig. 5. Due to the vacuum heating there is no essential compression of the ion as it is in the case of a normal incident-pulse laser [5]. The accelerated ions are mainly F^{8+} (H-like) ions at $I=2\times10^{18}\,\mathrm{W/cm^2}$ and F^{9+} at $I=4\times10^{18}\,\mathrm{W/cm^2}$ because of rapid ionization by the field. Inside the plasma, ions are mainly produced by collisional ionization, whereas in the surface region of the plasma OFI dominates. To verify the appearance of He-like and H-like ions among other accelerated ions, we make an estimation of the OFI by using Eq. (3). The time of ionization up to He-like ions by the field (for Li-like ion of fluorine $I_Z = 185\,\mathrm{eV}$) is less than 10 fs for laser intensity of $10^{18}\,\mathrm{W/cm^2}$. The time of field ionization for He-like ions is longer than the laser-pulse duration at this intensity. It means that ions in the plasma corona are rapidly ionized up to He-like and H-like states by the laser field. The OFI also lessens the level population of accelerated H- and He-like ions during the laser pulse. The field ionization from $2s$ and $2p$ levels of F^{8+} takes 10 fs, so that the He_α and He_β emissions by accelerated ions can appear only due to the pumping by hot electrons after laser pulse and, hence, represent the ion velocity distribution after laser pulse. The calculated plasma ionization is in good agreement with the estimation. In the skin layer for lower intensity there are H-like and He-like ions while ions in the bulk plasma are F^{5+} ions. Ionization waves are clearly seen in the bulk of the plasma. We assume that these waves are a result of the return current in the bulk plasma. Having lower energy than beamlike fast electrons produced by the vacuum heating and ponderomotive force, electrons in the return current can ionize more efficiently. For higher intensity there are fully ionized fluorine ions in the skin layer, while ions in the bulk plasma are F^{7+} (He-like) ions. The spatial distribution of the electron temperature is shown in Fig. 6. The maximal electron temperature is about 1.3 keV for lower intensity and increases only up to 1.7 keV for higher intensity because the laser energy deposited to fast electrons is rapidly spread over the plasma. The electron

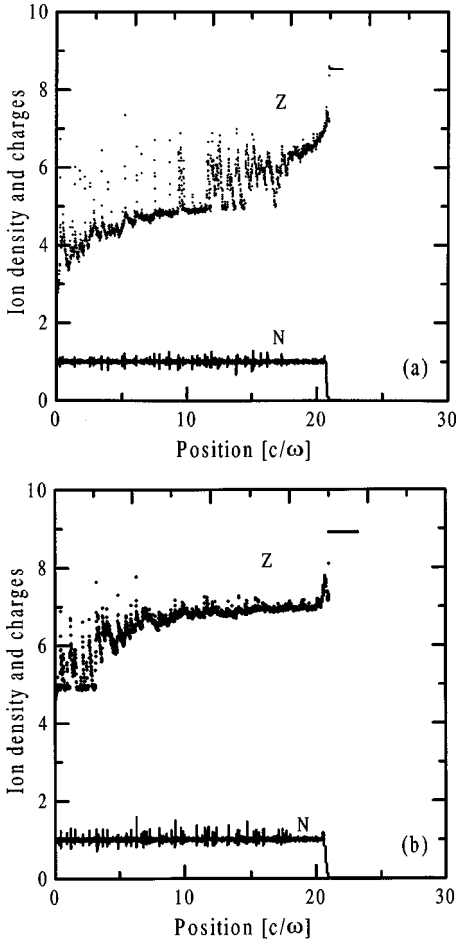

FIG. 5. Spatial ion density and charges distribution in the solid target after laser pulse (a) $I=2\times10^{18}\,\mathrm{W/cm^2}$ and (b) $I=4\times10^{18}\,\mathrm{W/cm^2}$.

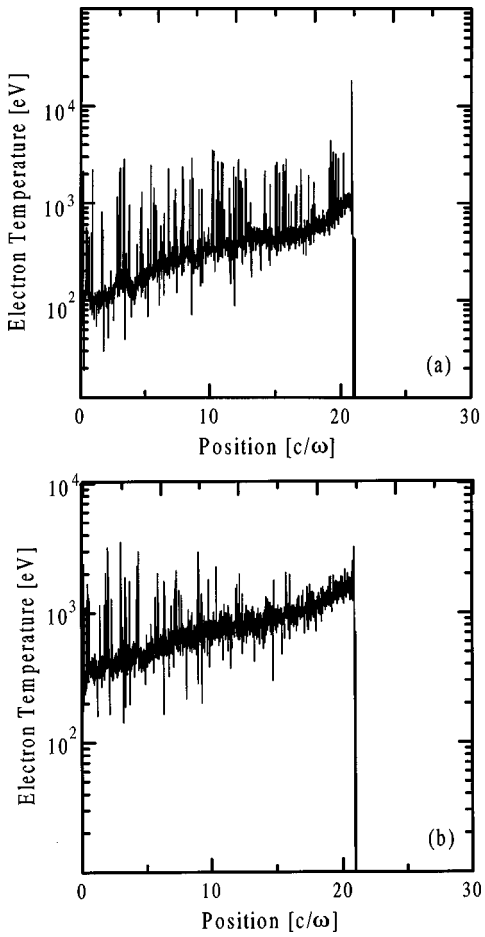

FIG. 6. Spatial distribution of the plasma temperature after laser pulse in the solid target (a) $I=2\times10^{18}\,\mathrm{W/cm^2}$ and (b) $I=4\times10^{18}\,\mathrm{W/cm^2}$.

temperature in the skin layer obtained from the PIC simulation is close to the temperature evaluated from the red wing of the spectra under assumption of the Doppler broadening.

The spatial distribution of accelerated ions after laser pulse is presented in Fig. 7. The velocity is close to a linear

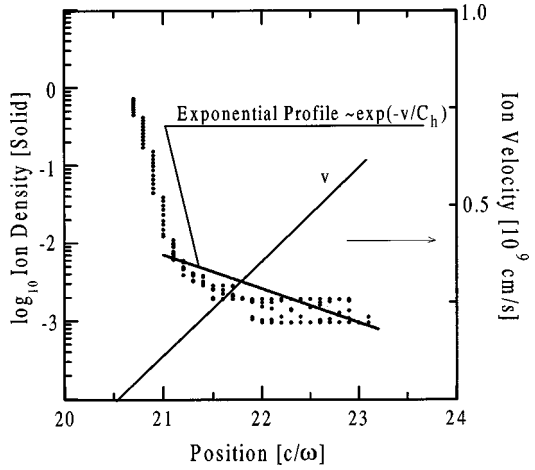

FIG. 7. Spatial distribution of velocity and density of accelerated ions after laser pulse from the solid surface at $I=4\times10^{18}\,\mathrm{W/cm^2}$. The fitting curve is the self-similar ion density with the ion sound speed C_h at $T_h=100\,\mathrm{keV}$.

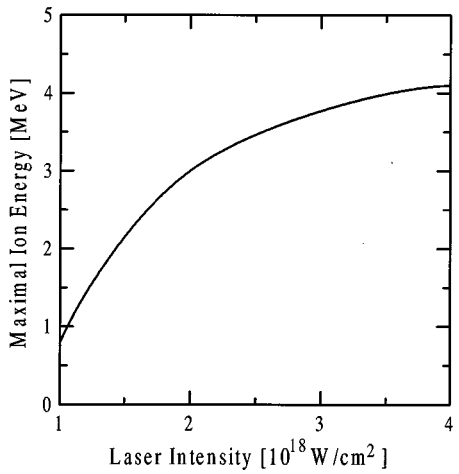

FIG. 8. Dependence of maximal ion energy on the intensity of the laser pulse.

distribution with the exponential density profile that corresponds to the self-similar plasma expansion with the ion sound speed determined by the temperature of hot electrons about 100 keV and justifies the estimation of ion velocity made above. In spite of only 0.5% of the laser energy being deposited to ions because the pulse laser is short, the maximal ion energy is over MeV (Fig. 8) and nonlinearly increases with the laser intensity exceeding the ponderomotive potential. A good agreement of the $1s3p$-$1s^2(\mathrm{He}_\beta)$ line shape with the line shape of Eq. (2) and the line shape calculated by using velocity distribution of accelerated ions from the PIC simulation is shown in Fig. 9.

In this calculation we neglected the presence of carbon ions in the experiment. But this can not affect the main results. Because the ionization potential of He-like carbon is twice as much as that of Li-like fluorine, the He-like carbon and He-like fluorine are mainly accelerated. The charge to atom mass ratio for F^{7+} (0.368) is greater than that for C^{4+} (0.333), so that the fluorine ions are accelerated faster.

The radiation of Stark-broadened H- and He-like ions from the solid density bulk plasma that in principle, can change the spectral distribution in the blue wing, is not included in the model either. We assume that the effect is

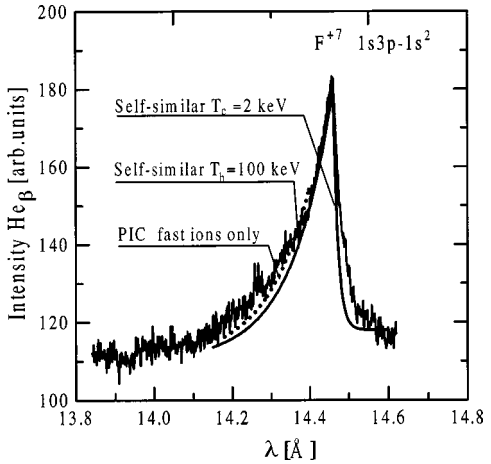

FIG. 9. Spectra of He_β. Curves are the spectra obtained with the self-similar distribution of fast ions and from the PIC simulation.

small because the laser pulse is very short in comparison with the time of radiative decay for all lines. The rapid cooling after the laser pulse due to the heat transfer inward the target leads to a very small population of $2p$, $3p$ levels of H- and He-like ions. In the solid density cold plasma, excited ions will be predominantly quenched by collisions rather than by radiative decay because the ratio $A/(VN_e)$ is small $(\sim 10^{-4})$, where A is the radiative decay rate and V is the collisional quench rate. The opacity decreases the effect of the bulk plasma on the time-integrated spectrum.

IV. CONCLUSION

We have demonstrated via the direct spectroscopic measurement and the PIC simulation the ion acceleration over MeV energies by an intense femtosecond *p*-polarized pulse laser. Due to the OFI the accelerated ions are He-, H-like, and fully ionized ions of fluorine. The line broadening is dominated by the distribution of the ion fluid velocity, which is close to the self-similar distribution. The spectral lines of accelerated ions show the clear asymmetric spectra. The blue wing is determined by the temperature of electrons that dominate the backward ion acceleration. This temperature is close to the well-known temperature of superthermal electrons. The temperature inferred from the red wing is close to the plasma temperature T_c. The spectral measurement can provide direct estimation of hot electron temperature T_h and T_c in the short intense pulse laser interaction with plasmas.

ACKNOWLEDGMENT

This work was partially supported by INTAS under Research Grant No. N 97-2090.

[1] W. L. Kruer and S. C. Wilks, Plasma Phys. Controlled Fusion **34**, 2061 (1992).
[2] R. Shepherd *et al.*, J. Quant. Spectrosc. Radiat. Transf. **58**, 911 (1997).
[3] E. P. Liang *et al.*, Phys. Rev. Lett. **81**, 4887 (1999).
[4] S. Miyamoto *et al.*, J. Plasma Fusion Res. **73**, 343 (1997).
[5] J. Denavit, Phys. Rev. Lett. **69**, 3052 (1992).
[6] A. Zhidkov, A. Sasaki, and T. Tajima, J. Plasma Fusion Res. (to be published).
[7] A. P. Fews *et al.*, Phys. Rev. Lett. **73**, 1801 (1994).
[8] J. Denavit, Phys. Rev. Lett. **69**, 3052 (1992).
[9] W. S. Lawson, P. W. Rambo, and D. J. Larson, Phys. Plasmas **4**, 788 (1997).
[10] S. Dobosz *et al.*, Zh. Eksp. Teor. Fiz., Pis'ma Red. **68**, 566 (1998) [JETP Lett. **68**, 592 (1998)].
[11] F. B. Rosmej *et al.* (unpublished).
[12] A. Ya. Faenov *et al.*, Phys. Scr. **50**, 333 (1994).
[13] T. Pikuz *et al.*, J. X-Ray Sci. Technol. **5**, 323 (1995).
[14] I. Yu. Skobelev *et al.*, Zh. Eksp. Teor. Fiz. **108**, 1263 (1995) [JETP **81**, 692 (1995)].
[15] B. K. F. Young *et al.*, Rev. Sci. Instrum. **69**, 4049 (1998).
[16] G. Hoelzer *et al.*, Phys. Scr. **57**, 301 (1998).
[17] S. J. Gitomer *et al.*, Phys. Fluids **29**, 2679 (1986).
[18] J. S. Pearlman and R. L. Morse, Phys. Rev. Lett. **40**, 1652 (1978).
[19] D. W. Forslund, J. M. Kindel, and K. Lee, Phys. Rev. Lett. **39**, 284 (1977).
[20] K. Estabrook and W. L. Kruer, Phys. Rev. Lett. **40**, 42 (1977).
[21] A. Zhidkov and A. Sasaki, Phys. Rev. E **59**, 7085 (1999).
[22] L. Landau and E. Lifshitz, *Quantum Mechanics* (Pergamon Press, New York, 1964), Vol. 3.
[23] M. V. Amosov, N. B. Delone, and V. P. Krainov, Zh. Eksp. Teor. Fiz. **91**, 2008 (1986) [Sov. Phys. JETP **64**, 1191 (1986)].
[24] S. C. Rae and K. Burnett, Phys. Rev. A **46**, 1084 (1992).
[25] F. Brunel, Phys. Fluids **31**, 2714 (1988).